Armenian Journal of Physics, 2013, vol. 6, issue 3, pp. 123-131

LONGITUDINALLY AND TRANSVERSELY POLARIZED TARGETS IN THE HERMES EXPERIMENT

H. H. MARUKYAN

A.I. Alikhanian National Laboratory (Yerevan Physics Institute),
Yerevan, Armenia
e-mail: marukyan@mail.desy.de

Received 1 July 2013

The nuclear-polarized hydrogen and deuterium targets have been used in HERMES experiment since the year 1996 until the end of the year 2005 with the polarized positron or electron beams of HERA electron storage ring at DESY to study the spin structure of the nucleon. The main characteristics and the performance of these targets during different periods of their operation are presented. The different mechanisms of gas depolarization active in the cell are presented and an evaluation of their effect on the final target polarization is given.

1. Introduction

Studies of quark-gluon spin structure of the nucleon have been carried out at HERMES by deeply inelastic scattering of longitudinally polarized leptons off a polarized internal gas target [1]. The structure functions g_1^p, g_1^n and g_1^d have been measured [2], first measurement of the structure function b_1^d [3], measurements of quark-flavour decomposition of the nucleon spin [4-7] have been performed. First measurements of single-spin asymmetries on longitudinally [8-10] and transversely polarized targets [11-14], as well as the study of gluon polarization also should be mentioned [15]. Besides, the amplitudes of azimuthal asymmetries in deeply virtual Compton scattering on longitudinally or transversely polarized hydrogen target [16-18], and longitudinally polarized deuterium target [19] have been measured.

Since the year 1996 until the end of the year 2005, the target was operated with both longitudinally polarized hydrogen ($H_\parallel$, 1996-1997) and deuterium ($D_\parallel$, 1998-2000), and transversely polarized hydrogen ($H_\perp$, 2002–2005) [20].

2. Target setup

The layout of the main elements of longitudinally polarized target is presented schematically in Fig. 1. The beam of H (D) atoms are formed by means of a radio-frequency (RF) or microwave (MW) dissociator, which was one of the main components of an atomic beam source (ABS) [21].

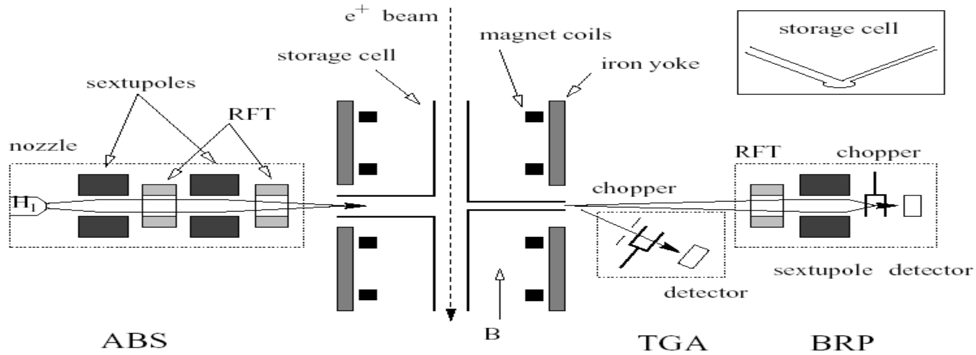

Fig. 1. A schematic view of the HERMES longitudinally polarized target. From left to right: atomic beam source (ABS), target chamber with cell, magnet and diagnostic system consisting of target gas analyzer (TGA) and Breit-Rabi polarimeter (BRP). The located radio-frequency transition (RFT) units are also shown.

After passing the system of sextupole magnets, the atoms became electron polarized by means of the process of Stern-Gerlach separation. Further, using two available sets of adiabatic high frequency transitions, the electron polarization transferred to the nucleons. The beam of nuclear-polarized atoms was injected into the center of the thin-walled storage cell via the side tube and was diffused to the open ends of the cell by means of a high-speed pumping system. The target cell is made of a 40 cm long aluminum tube of elliptical cross-section, coated with Drifilm [22], which enabled to minimize the depolarization effects due to the collision of atoms with the cell walls. Note that the usage of a cell with smaller cross-section (21x8.9 $мм^2$) after the year 1999 compared to that used before (29x9.8 $мм^2$) allowed increase the density of the target gas by 40%. The cell was mounted in a magnetic holding field. The target magnet provided the quantization axis for the spins of polarized atoms and simultaneously decoupled the magnetic moments of electrons and nucleons (see Fig. 2).

During the period of exploitation of the target in 1996–2000 the longitudinal magnetic field of about 330 mT was maintained by superconducting magnetic coils, while starting from the year 2001 the transverse field in the cell was provided by means of a dipole magnet specially made for this purpose.

A second side tube, the so-called sample tube, was intended for the selection of the gas from the cell center. It was used for the analysis of the atomic and molecular contents of the gas by means of a target gas analyzer (TGA) [23], as well as the polarization of atoms, which was defined from the measurement of relative populations of different hyperfine states in a Breit-Rabi polarimeter (BRP) [24].

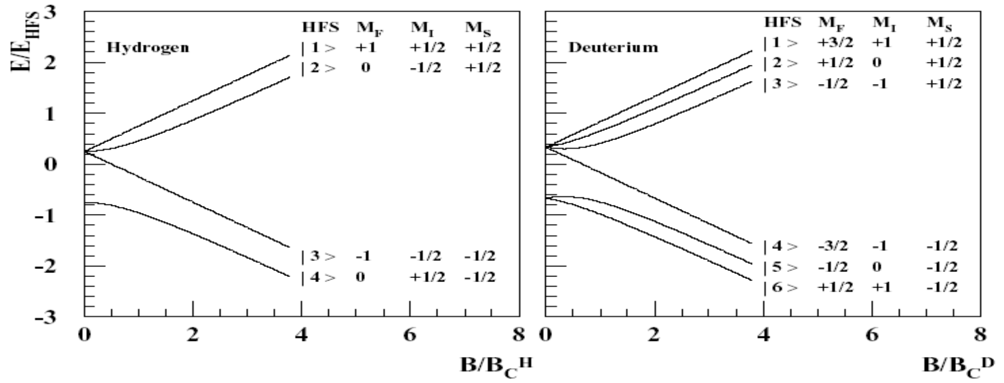

Fig. 2. Hyperfine energy levels of hydrogen (left panel) and deuterium (right panel) versus the magnetic holding field (Breit–Rabi diagram). The field values are given in units of corresponding critical field values.

3. Depolarization effects inside the cell

The main problem with the internal targets used at the storage rings is the nucleon depolarization that occurs due to different physical processes taking place inside the target [25]. Therefore, it is important to understand and evaluate the impact of these processes in order to reduce the systematic uncertainty in the measurement of the target polarization. These processes can be divided into two categories: recombination and spin relaxation processes. Atoms may recombine into molecules interacting with the surface of the storage cell walls or by colliding with other atoms in the gas volume. The volume recombination can be neglected due to the fact that the density of the gas used in the HERMES experiment was low. As the target was operated at temperatures below 140 K, the water worked out from the dissociator of the ABS formed an ice layer, which in turn reduced the probability of recombination of atoms on the surface of the cell. Thus, the effect of recombination actually was small and suppressed as much as possible.

Three different spin relaxation mechanisms led to depolarization of atoms, namely: depolarization, which occurs after collision of atoms with the cell walls; depolarization due to the spin-exchange process, when two atoms collide in the gas volume; resonant depolarization caused by high frequency fields induced by lepton beam bunches. The latter was a consequence of the interaction of transient magnetic field of the beam leptons with polarized target atoms. By applying an adequately strong magnetic field, the contribution to the depolarization that occurs from the first two mechanisms can be greatly reduced. The third mechanism can be avoided requiring a high uniformity of the target magnetic field.

The resonant depolarization was manifested when the lepton beam induced RF-harmonic coincide with the frequency difference between two different hyperfine states existing in the target. The probability of such a process is proportional to the square of the beam current. To determine the values of the magnetic field of the target at which this mechanism took place, it was necessary to investigate the time dependent RF-harmonic structure of the beam induced magnetic field. The distance between two bunches of the beam at the HERA was τ = 96 ns, so the frequency interval between the two harmonics is defined as $\upsilon = 1 / \tau$ = 10.41 MHz. Since the beam width of the bunch was very small (σ_t = 37.7 ps), this led to the fact that a large number of harmonics with non-zero amplitudes contributed to the induced RF-field. Fig. 3 shows the location of the depolarizing resonances, depending on the magnitude of the magnetic field for hydrogen and deuterium targets. Based on the results, the working area of the field of the target magnet (the area between the vertical lines in Fig. 3) was chosen.

Depending on a pair of hyperfine states selected with the ABS, it was possible to distinguish between the two types of transitions π and σ. The first one occurred when the RF-field component was perpendicular to the constant field supported within the cell $\Delta M_F = 1$, while the transition from σ $\Delta M_F = 0$ appeared when the above two fields were parallel. In the case of longitudinal polarization the field strength was $B_{\|}$=335 mT, and since the distance between the adjacent π resonances around a given working point is large, then it is not so difficult to exclude these resonances. For this reason, it was enough to ensure the uniformity of the longitudinal field at one percent level. For the σ resonances, which could only be detected in case of transverse holding field [26], the distance between them was only 0.37 mT, and it was necessary to ensure the field uniformity of the order of $\Delta B_{\perp} \leq 0.14$ mT.

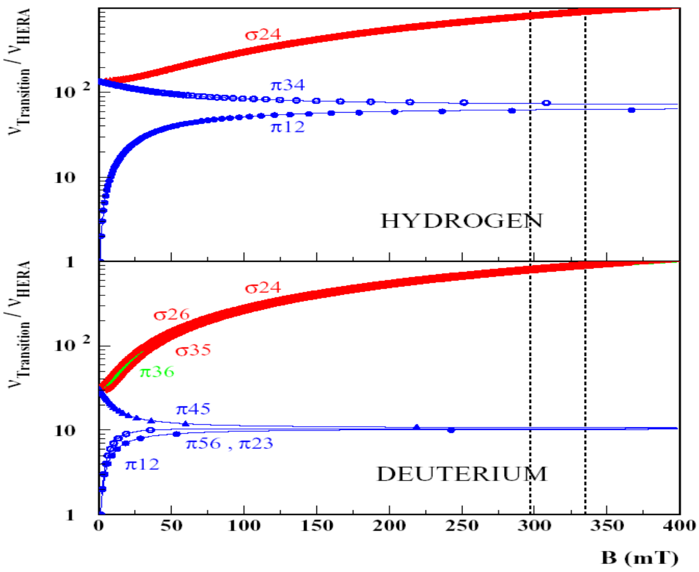

Fig. 3. Possible beam-induced nuclear depolarization resonances in the HERMES target.

Because of the geometry of the setup, it was technically difficult to design a transverse magnet so that it could fully satisfy the above requirement. Nevertheless, field uniformity was improved by adding additional ferromagnetic plates of a certain thickness installed in different locations along the magnet pole tips. It was found that the intensity of the field results in $B_\perp = 297$ mT, $\Delta B_\perp^z = 0.05$ mT, $\Delta B_\perp^y = 0.15$ mT and $\Delta B_\perp^x = 0.60$ mT, where the z component is directed along the axis of the magnet, which coincides with the direction of the beam leptons. Since the values of $\Delta B_\perp^x$ did not satisfy the necessary condition of homogeneity, a pair of additional correction coils along the target cell was used, made of special wire with independent power supply. As a consequence of this, the uniformity in the x direction was reached up to 0.2 mT. Due to the temperature increase of the magnet pole tips, the magnetic flux density was unstable during the operation. To overcome this, a system of automatic stabilization of the strong magnetic field was formed with a feedback based on the measurement of the magnetic flux density by means of a Hall sensor [27]. Gradually increasing currents were supplied to the coils of these additional rings around the magnet poles, according to the current reading of the sensor, to support the flux density of the magnet at the required level.

4. Characteristics of the targets

The average target polarization can be given by the following equation:

$$P^T = \alpha_o [\alpha_r + (1 - \alpha_r) \beta] P_a, \tag{1}$$

where α_o denotes the initial fraction of nuclei in the atoms of the gas injected by the ABS into the cell, α_r the fraction of nuclei in atoms that have escaped recombination, P_a the nuclear polarization of the atoms, $\beta = P_m/P_a$, where P_m represents the nuclear polarization of the molecules that are formed as a result of recombination of the atoms.

The values for α_o were calculated using the results of measurements of atomic and molecular composition of the gas in the TGA in combination with data from the different calibration measurements. P_a and α_r were determined from the polarization values and the fractions of nuclei in the atoms measured respectively in BRP and TGA, additionally taking into account for certain corrections. The latter was associated with the fact that both detectors were analyzing properties of only part of the target gas, which was taken directly from the center of target cell. The above corrections were calculated with the help of Monte Carlo simulations or determined analytically by using a one-dimensional diffusion equation [28]. Molecular polarization value was measured by using data on longitudinally polarized hydrogen and found to be $\beta = 0.64 \pm 0.19$ [29].

As an example, Fig. 4 shows the behavior of the target polarization during the 2005 running period. In this figure a clear difference in the level of polarization for two different cells is seen. The low polarization for the first one was due to repeated heating of the target, which was related with the problems in the cryogenic system.

Tables 1 and Table 2 summarize the main characteristics of longitudinally and transversely polarized targets, respectively.

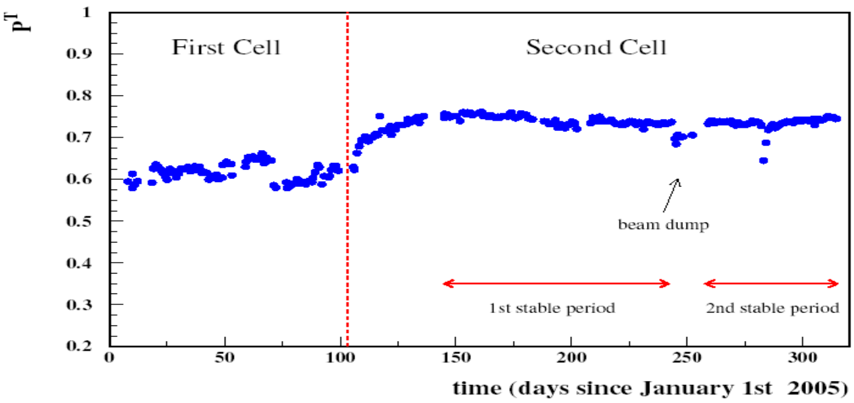

Fig. 4. The behavior of target polarization measured during 2005 running period.

In addition to the average polarizations, the tables also include such features as the degree of recombination $\Delta\alpha_r$=1-α_r, the degree of depolarization due to different polarization phenomena: spin-exchange collisions (ΔP_{SE}), depolarization due to collisions with the surface of the cell walls (ΔP_{WD}) and the resonant depolarization (ΔP_{BI}). Also the areal density of the target t and the relative factor of merit (FOM), which takes into account both the polarization and the density of the target for each cell, are given.

It should be noted that in the case of longitudinally polarized deuterium target in 2000, starting at a particular time, it was operated in a mode with combined vector and tensor polarizations instead of a normal selection mode of positive or negative vector polarization state. Tensor polarization components had a value equal to Pzz_+^T = 0.891 ± 0.027 and Pzz_-^T = -1.656 ± 0.049, respectively.

Unlike the case of hydrogen target, where the positive and negative components of the polarization vector exactly coincided in absolute value, for the deuterium target they were slightly different and were found to be P_{z+}^T = 0.851 ± 0.029 and P_{z-}^T = -0.840 ± 0.026, respectively. This difference was due to the presence of a larger number of efficiencies and transmissions involved in the calculation of the deuteron polarization [15] compared to those for the hydrogen. Note that in both tables only the systematic uncertainties of the polarization measurement are presented, as the statistical errors are small and can be neglected.

Table 1. Averaged characteristics for the longitudinally polarized hydrogen and deuterium targets in 1997 and 2000.

Target/year	H(1997)	D(2000)
P^T	0.851±0.033	0.845±0.028
$\Delta\alpha_r$	0.055	0.003(Absent)
ΔP_{SE}	0.035	≤0.001
ΔP_{WD}	0.020	≤ 0.01
ΔP_{BI}	Absent	Absent
t, 10^{14}nucleon/cm^2	0.7	2.1
FOM[$(P^T)^2$ t]	0.5	1.5

Table 2. Averaged characteristics for the transversely polarized hydrogen target in 2002–2005.

Target/year	08/2002 02/2003	10/2003 03/2004	04/2004 07/2004	01/2005 04/2005	04/2005 11/2005
P^T	0.780±0.050	0.786±0.036	0.721±0.050	0.620±0.090	0.730±0.060
$\Delta\alpha_r$	0.022	Absent	Absent	0.24	0.035
ΔP_{SE}	0.055	0.035	≤0.001	0.055	0.055
ΔP_{WD}	0.055	0.055	0.12	0.17	0.12
ΔP_{BI}	0.01	≤0.01	≤0.01	≤0.01	≤0.01
t,10^{14}nucleon/cm^2	1.1	1.1	1.1	1.1	1.1
FOM[$(P^T)^2$ t]	0.7	0.7	0.6	0.4	0.6

5. Discussion

Analysis of characteristics of longitudinally polarized hydrogen and deuterium targets showed that for the approximately same value of the magnetic holding field the spin-exchange process and the spin relaxation process on the target cell walls was suppressed about 20 times in the case of deuterium compared with the hydrogen.

From the Table 1, one can see that the target performance for $D_{\parallel}$ in 2000 was the most optimal one due to the absence of recombination ($\Delta\alpha_r \approx 0$) and a small depolarization quantity inside the target ($\Delta P_{SE} \approx \Delta P_{SE} \approx 0$). This was the consequence of the fact that the critical field value for the deuterium is 11.7 mT, which is much lower than the critical field for the hydrogen - 50.7 mT. Besides, by applying a quality coating on the surface of the cell, based on the previous experience of operating targets, improved the cell performance.

Reducing the percentage of surface recombination inside the cell for the target H⊥ in 2002 (see Table 2), compared with $H_{\|}$ in 1997 (see Table 1), was also due to the improvement of the aforementioned coating. On the other hand, effects of spin relaxation in 2002 were more significant because of the relatively high density and a greater number of collisions with the walls, leading to the reduction of polarization by about 11%. Because of this, the increase in FOM, due to an increase in the integrated density of the gas, was limited compared with the year 1997.

6. Summary

Since 1996 until the end of 2005, longitudinally and transversely polarized hydrogen, as well as longitudinally polarized deuterium target efficiently and reliably operated in the experiment HERMES. They provided the gas density of the order of 1-2x10^{14} nucleon/cm^2, a high degree of polarization in the range of 0.72 - 0.85, with a total uncertainty of the order of 0.03 - 0.04. Contributions from the processes of recombination and depolarization in the systematic error were fully under control. How well the target can be controlled was confirmed also indirectly by the first measurement of hydrogen spin-exchange collision cross section in the low temperature region 40-100 K [30], which was performed at HERMES in an experiment taken during the period when HERA did not operate.

References

1. HERMES Technical Design Report, DESY-PRC 93/06, 1993.
2. A. Airapetian, N. Akopov, …, **H. Marukyan** et al., submitted to Phys. Rev. D 75 (2007) 012007.
3. A. Airapetian, N. Akopov, …, **H. Marukyan** et al., Phys. Rev. Lett. 95 (2005) 242001.
4. K. Ackerstaff, A. Airapetian, …, **H. Marukyan** et al., Phys. Lett. B 464 (1999) 123.
5. A. Airapetian, N. Akopov, …, **H. Marukyan** et al., Phys. Rev. Lett. 92 (2004) 012005.
6. A. Airapetian, N. Akopov, …, **H. Marukyan** et al., Phys. Rev. D 71 (2005) 012003.
7. A. Airapetian, N. Akopov, …, **H. Marukyan** et al., Phys. Lett. B 666 (2008) 446.
8. A. Airapetian, N. Akopov, M. Amarian et al., Phys. Rev. Lett. 84 (2000) 4047.
9. A. Airapetian, N. Akopov, …, **H. Marukyan** et al., Phys. Lett. B 562 (2003) 182.
10. A. Airapetian, N. Akopov, …, **H. Marukyan** et al., Phys. Lett. B 622 (2005) 14.
11. A. Airapetian, N. Akopov, …, **H. Marukyan** et al., Phys. Rev. Lett. 94 (2005) 012002.
12. A. Airapetian, N. Akopov, …, **H. Marukyan** et al., JHEP 06 (2008) 017.
13. A. Airapetian, N. Akopov, …, **H. Marukyan** et al., Phys. Rev. Lett. 103 (2009) 152002.
14. A. Airapetian, N. Akopov, …, **H. Marukyan** et al., Phys. Lett. B 693 (2010) 11.
15. A. Airapetian, N. Akopov, …, **H. Marukyan** et al., JHEP 08 (2010) 130.
16. A. Airapetian, N. Akopov, …, **H. Marukyan** et al., JHEP 06 (2010) 019.
17. A. Airapetian, N. Akopov, …, **H. Marukyan** et al., Nucl. Phys. B 842 (2011) 265.
18. A. Airapetian, N. Akopov, …, **H. Marukyan** et al., JHEP 06 (2008) 066.

19. A. Airapetian, N. Akopov, …, **H. Marukyan** et al., Phys. Lett. B 704 (2011) 15.
20. A. Airapetian, N. Akopov, …, **H. Marukyan** et al., Nucl. Instr. and Meth. A 540 (2005) 68.
21. A Nass, C. Baumgarten,…, **H. Marukyan** et al., Nucl. Instr. and Meth. A 505 (2003) 633.
22. C. Baumgarten, B. Braun,…, **H. Marukyan** et al., Nucl. Instr. and Meth. A 496 (2003) 277.
23. C. Baumgarten, B. Braun,…, **H. Marukyan** et al., Nucl. Instr. and Meth. A 508 (2003) 268.
24. C. Baumgarten, B. Braun, G. Court et al., Nucl. Instr. and Meth. A 482 (2002) 606.
25. C. Baumgarten, Ph. D. Thesis, Ludwig-Maximilians Universitaet, Munchen, May, 2000.
26. W. Sig-uang, , Z. Shu-Hua,…, **H. Marukyan** et al., High Energy Phys. and Nucl. Phys., China, 30, N9, 892-895, 2006.
27. W. Siguang, M. Boumwhuis,…, **H. Marukyan** et al., Nulear Techniques, China, 28, N4, 297-300, 2005.
28. C. Baumgarten, B. Braun, G. Court et al., Eur. Phys. J. D 18 (2002) 37.
29. A. Airapetian, N. Akopov, …, **H. Marukyan** et al., Eur. Phys. J. D 29 (2004) 21.
30. C. Baumgarten, B. Braun,…, **H. Marukyan** et al., Eur. Phys. J. D48, 343-350, 2008.